Chemical control of the electrical surface properties in donor-doped transition metal oxides

M. Andrä,[1,2,*] H. Bluhm,[3] R. Dittmann,[1,2] C. M. Schneider,[2,4,5] R. Waser,[1,2,6] D. N. Mueller,[2,4,†] and F. Gunkel[1,2,6,‡]

[1]*Peter Grünberg Institute 7, Forschungszentrum Juelich GmbH, Juelich, Germany*

[2]*Juelich Aachen Research Alliance for Fundamentals on Future Information Technology (JARA-FIT), Juelich, Germany*

[3]*Chemical Sciences Division, Lawrence Berkeley National Laboratory, 1 Cyclotron Road, Berkeley, California 94720, USA*

[4]*Peter Grünberg Institute 6, Forschungszentrum Juelich GmbH, Juelich, Germany*

[5]*Physics Department, University of California, Davis, California 95616, USA*

[6]*Institut für Werkstoffe der Elektrotechnik II, RWTH Aachen University, Aachen, Germany*

(Received 21 August 2018; published 15 April 2019)

Donor-doped transition metal oxides such as donor-doped strontium titanate (n-$SrTiO_3$) are of fundamental importance for oxide electronic devices as well as for electronic surface and interface engineering. Here we quantitatively analyze the variable band alignment and the resulting space charge layer at the surface of n-$SrTiO_3$, determined by its surface redox chemistry. Synchrotron-based ambient-pressure x-ray photoelectron spectroscopy conducted under applied thermodynamic bias is used to access electronic structure and chemistry of the surface. We find an electron depletion layer driven by cationic surface point defects that are controlled by adjusting the ambient atmosphere (pO_2). We correlate the pO_2 dependence to a response of the strontium sublattice, namely the precipitation of strontium oxide and the formation of charged strontium vacancies at the surface. We suggest the reversible conversion of surface-terminating strontium oxide into extended strontium oxide clusters as the responsible process by resolving chemical dynamics *in situ*. As we show, atomic control of these subtle changes in the surface redox chemistry allows us to tailor electrical transport properties along the n-$SrTiO_3$ surface. Our study thereby gives access to engineering electronic band bending in transition metal oxides by the control of the surface chemistry.

DOI: 10.1103/PhysRevMaterials.3.044604

I. INTRODUCTION

Perovskite-type transition metal oxides (TMOs) are of high scientific interest due to their variety of electrical and magnetic properties [1–4]. Especially their surface and interface properties and the strong coupling of lattice disorder and electronic structure give rise to a wide range of interesting effects and applications, such as resistive switching [5–8], the formation of two-dimensional electron gases [9–11], efficient solar cells [12], and solid oxide fuel cell electrodes [13,14]. In all cases, surface and interface properties are of the utmost concern, as they often influence or even determine device properties, by defining interface dipoles [15], band alignments [16,17], or space charge layers [18]. Understanding and actively tuning the electrical surface properties in TMOs is hence highly desirable.

As a typical model material, donor-doped strontium titanate (n-$SrTiO_3$) has gained significant attention. It is used for direct applications, such as gas sensors [19,20] or superconducting [21] and memresistive devices [7,22,23]. Moreover, n-$SrTiO_3$ is used as a quasimetallic substrate for superconducting thin films [24], ferroelectric tunnel junctions [25–27], oxidic water splitting catalysts [28], and resistive switching devices [6,7,29]. The bulk of n-$SrTiO_3$ is referred to as a degenerate n-type semiconductor. Ionic defect equilibria relevant to the lattice disorder of n-$SrTiO_3$ are often neglected due to their sluggish response times [30,31], rendering the bulk of n-$SrTiO_3$ a simple oxide semiconductor characterized by its extrinsic dopant concentration and the corresponding electron concentration.

Approaching nanoscale structures and devices such as thin films, heterostructures, and interfaces [9,32–36], however, electronic and ionic properties may differ from the known bulk behavior [18,31,37–40]. This is due to the reduced dimensions, the presence of space charges, built-in electric fields, or band bending and the small relevant diffusion lengths involved.

For n-$SrTiO_3$, there are indications of the existence of a surface space charge layer pointing towards a more complex behavior of the surface as compared to the bulk [22,32]. In a previous study, we have shown the presence of a surface space charge layer by laboratory-based ambient-pressure x-ray photoelectron spectroscopy (AP-XPS) [41]. In agreement with this, eased electronic transport and charge trapping in the vicinity of the surface was reported [22,32,42]. The origin of this surface space charge layer, however, has not been clarified yet. Possible scenarios considered are intrinsic surface states, ionic charges formed at the surface by adsorption of gas molecules [22,43,44], and ionic charges originating from Sr vacancy defects formed in the course of oxidation [31,42].

To clarify this, we address the redox chemistry of the n-$SrTiO_3$ surface, investigate its dependence on thermodynamic bias induced by a controlled oxygen atmosphere (pO_2),

*m.andrae@fz-juelich.de
†dav.mueller@fz-juelich.de
‡Gunkel@iwe.rwth-aachen.de

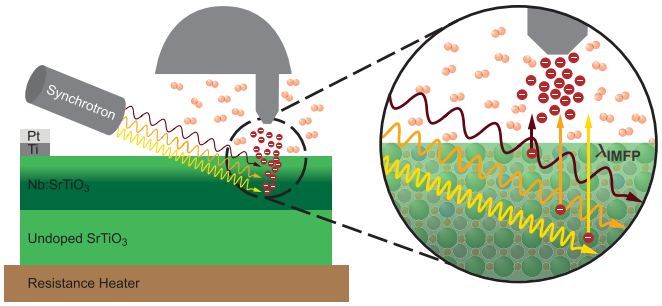

FIG. 1. Schematic illustration of the AP-XPS experiments enabling us to apply thermodynamic bias during the measurements. Using different incident photon energies the kinetic energy of excited electrons can be tuned, resulting in specific inelastic mean-free paths for a given core level. In this way, depth-resolved measurements in a controlled oxygen atmosphere are obtained.

and characterize the resulting surface band bending and electrical transport properties as a function of pO_2. For this, electronic structure and surface chemistry are accessed by AP-XPS carried out *in situ* with different incident photon energy and in different oxygen atmospheres (Fig. 1). Due to its tunable surface sensitivity, synchrotron-based AP-XPS allows us to elucidate changes in surface chemistry and electronic structure simultaneously. A controlled pO_2 during the experiment (up to 1.3 mbar O_2) allows us to follow the chemical response of the sample to a varied oxygen atmosphere. Elevated sample temperatures (670 K) activate ionic equilibria and allow for atomic rearrangements in response to the ambient atmosphere. Varying the incident photon energies, we achieve depth profiling, allowing us to track the potential profile of the space charge layer in different atmospheres. Spectroscopic analysis is complemented by electrical transport experiments carried out under comparable conditions, which consistently show a corroborating variation in electron density in the thin films as the surface chemistry is varied. In this way, we can link the chemical response and electronic structure of the surface to the electronic transport behavior. Based on the defect chemistry of n-$SrTiO_3$, we propose a surface redox process involving the formation of negatively charged Sr vacancy defects, kinetically confined to the surface and concomitant to the clustering of SrO precipitates, to cause the pO_2 dependence of the surface space charge layer in n-$SrTiO_3$.

II. SAMPLE PREPARATION AND EXPERIMENTAL DETAILS

We deposited stoichiometric 0.5 wt.% Nb-doped $SrTiO_3$ thin films by pulsed laser deposition on undoped single-crystalline $SrTiO_3$ (100) substrates (CrysTec GmbH, Berlin, Germany), using a KrF excimer laser ($\lambda = 248$ nm) with a laser fluence of 1.2 J/cm^2 at a repetition rate of 5 Hz, a spot size of 2 mm^2, and a target-to-substrate distance of 44 mm. The film was grown in an oxygen atmosphere of 0.1 mbar at a substrate temperature of 1073 K. The growth process was monitored by reflection high energy electron diffraction (RHEED). Clear RHEED intensity oscillations indicated a layer-by-layer growth of the thin film. After the growth the sample was quenched down to room temperature and no further treatment was performed prior to the different experiments. The quality of the stoichiometric growth process was analyzed carefully by atomic force microscopy (Cypher, Asylum Research), RHEED (see Sec. I of the Supplemental Material [72]), and Hall measurements (Lake Shore 8400 series).

In order to characterize the surface space charge layer and to clarify its origin we use synchrotron-based AP-XPS measurements applying variable x-ray photon energies at elevated temperature and in different oxygen atmospheres (beamline 11.0.2, Advanced Light Source, Berkeley, CA, USA) [45,46]. Figure 1 shows a schematic illustration of the experiment allowing direct access to the surface chemistry and electronic structure while applying a controlled oxygen pressure. The atmospheres applied *in situ* during the measurements ranged from 10^{-8} mbar base pressure up to 1.3 mbar oxygen atmosphere, which also defined the total pressure during the AP-XPS measurements. The elevated sample temperature (670 K) during the experiment allows us to activate ionic reactions at the surface. All characteristic core levels of n-$SrTiO_3$ (Sr 3d, O 1s, Ti 2p, and Sr 3p) were investigated. Variable incident photon energies yield different kinetic energies and thus inelastic mean-free paths (IMFPs) of excited core level electrons, allowing depth-resolved measurements (Fig. 1).

The as-prepared sample was contacted from the top using thin metal contact strips consisting of 50 nm platinum on top of 5 nm titanium deposited by e-beam evaporation. This way, an Ohmic contact between the n-$SrTiO_3$ thin film and the analyzer ground contact (Fermi coupling) is ensured. The photon energy was varied from 1080 eV to 270 eV. For Sr 3d core level spectroscopy, this corresponds to IMFPs ranging from 1.2 nm to 0.4 nm at the electron take off angle of 40°, as calculated by the TPP2M formula [47]. All binding energy scales are calibrated to the literature value of the Au 4f core level collected on a thin gold foil attached to the sample [48,49]. Note that this only corrects possible variations in the incident photon energy. A typical measurement took about 30 minutes to 1 hour to adjust and stabilize temperature and gas pressure, followed by about 24 hours to execute the spectroscopic experiments. During the entire time, the sample was kept under constant conditions. No transient changes in spectral shape or binding energy position were observed throughout the experiments, indicating spectroscopic equilibrium after the adjustments.

Electrical transport under varied oxygen atmospheres was measured in a 4-point probe setup, while exposing the sample to gas mixtures of equivalent pO_2 and a similar temperature to that applied in the AP-XPS experiments (670 K). The oxygen pressure in the electrical measurement was varied from 0.005 mbar O_2 to 1.0 mbar O_2 in a total pressure of 1.0 bar by using mixtures of argon gas with a purity of 6.0 and a premixed gas consisting of 0.1 % O_2 in Ar (Air Products and Chemicals, PRAXAIR). The transition between two gas atmospheres was realized quickly by premixing different pO_2 in two parallel flow channels and switching between them using a four-port valve. This way we could ensure that the switching of the ambient atmosphere can be regarded as instantaneous with respect to the timescale of the conductivity relaxation.

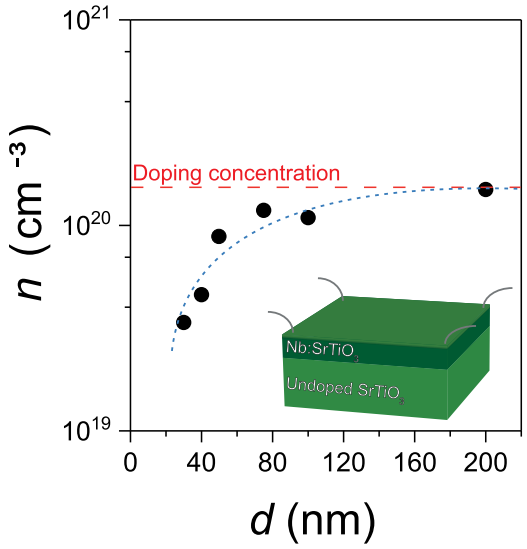

FIG. 2. Carrier concentration obtained for 0.5 wt.% n-$SrTiO_3$ thin films with different layer thicknesses. The red dashed line indicates the nominal donor concentration. The blue dashed line is a guide to the eye emphasizing the effect of electron depletion at low layer thicknesses.

III. RESULTS AND DISCUSSION

A. Surface electron depletion in as-prepared n-$SrTiO_3$ thin films

Figure 2 shows the carrier concentration obtained for n-$SrTiO_3$ thin films with different layer thicknesses as determined from room temperature Hall measurements immediately after synthesis. In an ideal semiconductor picture, one would expect a thickness-independent carrier density that matches the Nb-dopant concentration (1.5×10^{20} cm^{-3}, dashed line). In contrast, however, we observe a systematic thickness dependence of the electron density. Only at layer thickness approaching 200 nm the carrier concentration coincides with the donor concentration. At lower film thicknesses, however, the carrier concentration decreases significantly below the donor concentration. At a thickness of 30 nm, the conductivity of the thin films was even below the detection limit and no carrier concentration could be determined. The systematic decrease of the carrier concentration at small layer thicknesses below about 100 nm is indicative of an electron depletion layer becoming the dominant factor for electron transport. The as-grown layers hence readily form an inherent space charge layer, consistent with earlier reports [32]. A more trivial explanation for the observed thickness-dependent electron density is a nonideal growth process leading to the incorporation of defects and electron traps during synthesis [30,50–52]. However, growth-induced defects would be expected to become increasingly effective as the layer thickness increases. In Fig. 2, we observe opposite behavior: the carrier density approaches the Nb concentration with increasing layer thickness, indicating a stoichiometric synthesis process, and thus supporting the interpretation of an electron depletion layer present at the surface of the thin films. In analogy to semiconductors, the physical origin of this may be intrinsic surface states or unsaturated dangling bonds [32]. However, also ionic defect states or charged adsorbates can form localized negative charges, which would drive electron depletion [31,41,43,44]. A physical fingerprint of such a redox-chemistry-triggered effect is the characteristic dependence on the activity of the oxidizing agent. The key question arising from this is whether the observed electron depletion layer shows a characteristic dependence on pO_2 that can be identified as a physical fingerprint and allows for a controlled manipulation. This will be addressed below by synchrotron-based AP-XPS.

B. pO_2 dependence of space charge layer and surface chemistry

To investigate the surface redox-chemistry directly, we performed *in situ* spectroscopic experiments while varying the pO_2. The experimental conditions emulate those during thin-film synthesis, where elevated temperatures are applied and oxygen pressure is a major control parameter. Figure 3 shows (a) Sr 3d core level spectra measured at a temperature of 670 K in ultrahigh vacuum (UHV; 10^{-8} mbar) and at increased oxygen pressure (1.3 mbar O_2) (b) for different probing depths. The Sr 3d core level spectra shift systematically towards lower binding energies (BEs) with decreasing probing depth, as observed for both measurements in UHV and high pO_2 conditions [cf. dashed lines in Figs. 3(a), 3(b)]. A similar shift with varied probing depths is observed for all core level spectra (cf. Sec. II of the Supplemental Material [72]). This rigid shift of all spectra is indicative of electronic band bending within the probed volume and consistent with an electron depletion layer at the surface of the thin film [41]. It is noteworthy that the shifts observed in UHV [Fig. 3(a)] indicate that the electron depletion layer at the surface of n-$SrTiO_3$ is present not only when oxygen is applied, but also persists in (reducing) UHV conditions [53].

While spectral shifts along the energy axis indicate electronic band bending, chemical information is contained in the detailed shape of the core level spectra. In order to reveal chemical changes with varied probing depths and varied atmosphere, we superimposed the core level spectra artificially so that the maxima coincide, such as shown for Sr 3d, O 1s, and Ti 2p in Fig. 3, panels (c)–(h). For this, all energy scales were shifted to overlap the spectra, as denoted by the relative binding energy notation. The oxygen [(e), (f)] and titanium [(g), (h)] core levels barely show any changes in their spectral shape, neither with probing depth nor oxygen atmosphere. In contrast, the Sr 3d core level [(c), (d)] spectra shows significant changes in shape, indicating an altered Sr chemistry as the experiment becomes more and more surface sensitive. Together with the absence of any significant changes in the oxygen and titanium spectra, this clearly indicates that the Sr sublattice at the surface is involved in the surface-redox process.

In Fig. 4, we therefore focus on a detailed analysis of the Sr 3d spectra. All recorded Sr 3d spectra have the necessity to be described by two doublets, one of them attributed to a bulk component and one to a surface component, typically identified as SrO secondary phase [54–56], as shown in Figs. 4(a) and 4(b). Embedded into the data are now individual fits after a Shirley background subtraction, consisting of two Voigt doublets that represent the bulk component (at lower binding energy) and the surface component (at higher binding energy)

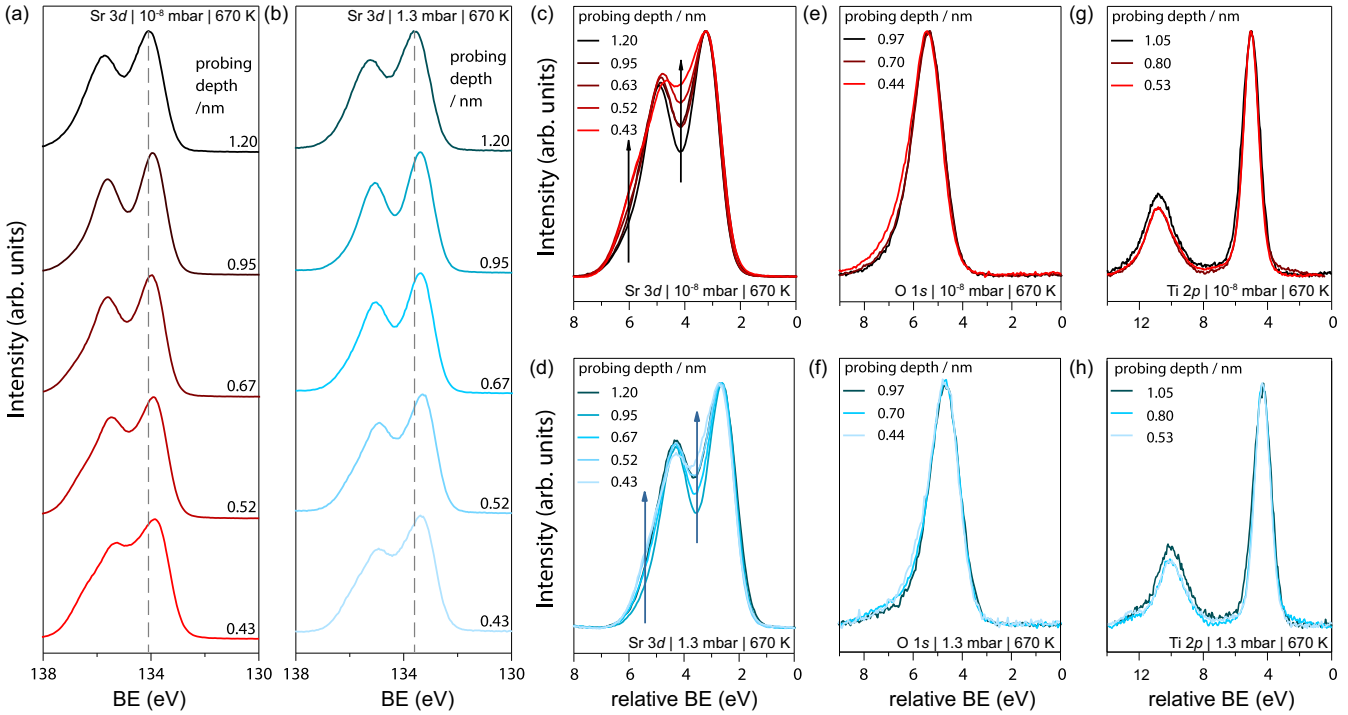

FIG. 3. AP-XPS data obtained for the Sr 3*d* core level spectra at different probing depths in UHV (10^{-8} mbar) (a) and high oxygen pressure of 1.3 mbar (b). In (c)–(h), the core level spectra obtained for Sr 3*d*, O 1*s*, and Ti 2*p* were superimposed. (c), (e), (g) display data obtained in UHV; (d), (f), (h) display data obtained at a pO_2 of 1.3 mbar. Note that for a more ready comparison in (c)–(h), the maxima of each core level were artificially shifted to coincide (relative binding energy scales), thereby removing the observed peak shifts.

separated by 0.8 eV along the energy axis [54]. In the fitting, we assumed the same Lorentzian width (natural linewidth), peak splitting, and area ratios for each doublet, but allowed different Gaussian widths to account for peak broadening induced by nonuniform potential distribution along the penetration depth [57]. All Sr 3*d* core level spectra obtained at different probing depths and oxygen atmospheres are described well by this fitting scheme. Figure 4(c) plots the binding energy positions of the bulk Sr $3d_{5/2}$ peaks (low binding energy component) obtained at different probing depths for the measurements in UHV and in oxygen. As already indicated in Fig. 3, the binding energy positions of the Sr 3*d* core level peaks shift towards lower values in more surface-sensitive measurements. In both atmospheres, the shift in binding energy with the probing depth is comparable (0.3 eV when varying the probing depth from 0.4 nm to 1.2 nm). The similar slopes observed in UHV and 1.3 mbar O_2 indicate comparable electric fields (≈4 MV/cm) associated with the space charge layer under both conditions. As a result of the varied oxygen atmosphere, however, the binding energies in oxygen and UHV are offset by 0.55 eV [58], indicating a significant shift of the Fermi level into the band gap when inducing oxidizing conditions [41,59]. This result is corroborated by the rigid shift of all other core levels (see Sec. II of the Supplemental Material [72]) when exposing the sample to oxygen atmosphere. Hence, in contrast to earlier reports [41], the responsible electron depletion layer is present both in UHV and in oxidizing conditions, but becomes much more pronounced as the surface is exposed to oxygen. Note that due to the present band bending, the peak positions observed in AP-XPS correspond to *apparent* binding energy positions, as each of the spectra is composed by a superposition of multiple peaks all offset along the binding energy axis. This makes the extraction of the real potential profile from the peak positions difficult [57] (for a more detailed discussion the reader is referred to Sec. III of the Supplemental Material [72]).

C. Control of electronic transport properties

A consistent result is found in electrical transport measurements carried out at similar temperature and under varied oxygen atmosphere. For the transport experiment, we used a 32 nm thick layer, for which the electrical properties are heavily dominated by the surface depletion layer, as indicated by the significantly decreased carrier density as compared to the nominal dopant concentration (Fig. 2).

Figure 5(a) illustrates a dynamic change of the electrical transport properties, as the ambient pO_2 is varied. The measurement took place at a temperature of 670 K after an instantaneous change in ambient atmosphere from 0.005 mbar up to 1 mbar and vice versa, which is comparable to the pressure range used for our *in situ* AP-XPS experiments, directly linking the results of the two independent experimental techniques (Sec. IV of the Supplemental Material [72] provides a more detailed comparison of the dynamics observed in the two experiments). Changing the ambient pO_2 at elevated temperatures immediately drives a reaction of the sheet resistance of the thin film. An increase of the pO_2 results in an increase of R_s while a subsequent decrease of the pO_2 results in a decrease of R_s. This means that at a temperature of 670 K the chemical response of the thin film (as probed by AP-XPS) results in an active variation of the carrier density

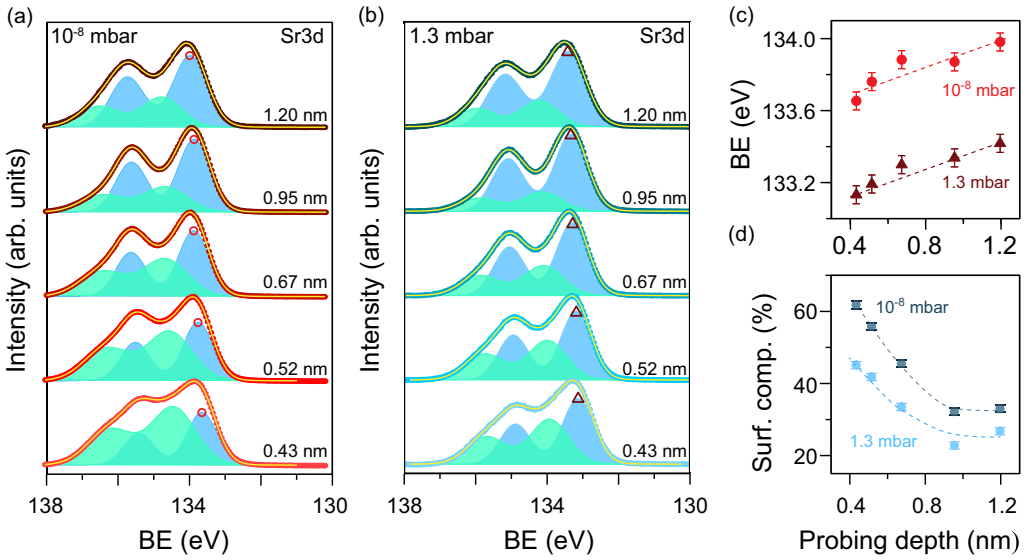

FIG. 4. Fitting of the Sr 3*d* spectra obtained in UHV (10^{-8} mbar) (a) and in high oxygen pressure of 1.3 mbar (b). Two doublets are required, attributed to a bulk contribution (dark area) and a surface contribution (light area), typically identified as SrO secondary phase. The data are displayed as red and blue circles; the orange lines indicate the envelope of the fit. In (c), we plot the actual peak positions obtained for the Sr $3d_{5/2}$ bulk component, as indicated by the red circles/triangles in (a) and (b). The relative area contribution of the surface component to the total core level area is shown in (d). Dashed lines represent guides to the eyes.

in the film. As displayed in Fig. 5(b), the equilibrium sheet resistance obtained after 12 h of equilibration at constant oxygen pressure increases when increasing the ambient pO_2 stepwise, indicating a continuously increasing effect of the electron surface depletion as the sample is exposed to higher oxygen concentrations.

The observed resistance change goes hand in hand with an altered sheet electron concentration ($n_S = [eR_s\mu(T)]^{-1}$). Here, $\mu(T)$ denotes the electron mobility, which was determined directly in high-temperature Hall measurements [$\mu(670\,\mathrm{K}) = 0.45\,\mathrm{cm}^2/\mathrm{Vs}$; see Sec. V of the Supplemental Material [72] for details)]. This allows us to convert the transient change in R_S into a transient change in electron density yielding the evolution of the average sheet carrier density in the *n*-$SrTiO_3$ thin film upon a change in pO_2 [lower panel of Fig. 5(a), blue]. The trend of n_s correlates directly to the formation of the more pronounced surface space charge layer observed in spectroscopy as the sample gets oxidized. The higher the ambient pO_2 the more the Fermi level is shifted into the band gap, resulting in a lower carrier concentration in the thin film; cf. Fig 4(c).

The corresponding band bending is characterized by a built-in electric field, which via the Gauss law is associated with a charge Q/A located at the surface of *n*-$SrTiO_3$. In order to quantitatively evaluate this surface charge from the electrical resistance measurements, we obtain Q/A as the difference of electron density contributing to transport (n_s) and the total amount of niobium dopants available in the thin film:

$$Q/A = n_s - N_D d_{layer}, \tag{1}$$

where d_{layer} denotes the thin-film thickness. The corresponding electric field at the surface is then given by

$$E = \frac{Q/A}{\varepsilon_0 \varepsilon_r}. \tag{2}$$

Table I summarizes the values determined using the equilibrium sheet electron concentrations obtained in 0.005 mbar and 1 mbar of oxygen [Fig. 5(a)]. The electric field at the surface obtained from this estimation is of order 4.3-4.4 MV cm^{-1}, which corresponds well with strong peak shifts observed at different probing depths in AP-XPS [Fig. 4(c)]. The corresponding surface charge yields −2.88 and -3.00×10^{14} $\mathrm{e/cm}^2$, respectively. Taking into account the dielectric constant of $SrTiO_3$ [$\varepsilon_r(670\ \mathrm{K}) = 122$] [31], a screening length on the order of 20 nm can be estimated. This screening length can explain the suppressed conductivity in thin films at a film thickness of up to 30 nm. The surface charge changes by 3.9% with the transition from low to high pO_2, while the sheet resistance changes by 6.7%. Hence, a small alteration of the pO_2 affects the electron transport along the surface of *n*-$SrTiO_3$ significantly.

D. Surface redox chemistry of *n*-$SrTiO_3$

The observed pO_2 dependence of the core level binding energies and of the electronic transport properties along the thin films cannot be explained by a classical surface potential caused by intrinsic surface states, as this would be expected to show no pO_2 dependence at all. Therefore, the observed behavior and particularly the evolution of Sr 3*d* spectral shape hints towards a more complex surface mechanism, involving the surface redox chemistry of *n*-$SrTiO_3$. In this case, two possible mechanisms have been suggested, implying either strontium vacancy formation or the presence of charged oxygen adsorbates at the surface [31,41,43]. In the latter case, it is unlikely to observe a strong response of the Sr core levels on pO_2, while no significant change is observed in O 1*s*. In contrast, this is a strong hint towards a Sr vacancy scenario. Here, we additionally probed the chemical bonding states at the surface quantitatively by evaluating the fits of the

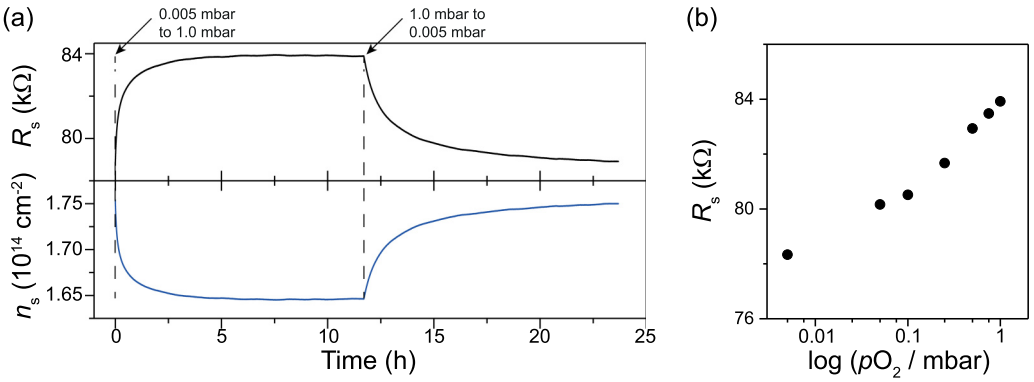

FIG. 5. (a) Reversible change in sheet resistance (R_s, black) and sheet electron density (n_s, blue) in response to an abrupt change in ambient oxygen atmosphere (5×10^{-3} mbar → 1 mbar → 5×10^{-3} mbar), as determined for a 32 nm thick 0.5 wt.% *n*-$SrTiO_3$ thin film at 670 K. (b) Equilibrium resistance obtained after 12 h of equilibration in a defined oxygen pressure as a function of oxygen partial pressure (pO_2).

Sr 3*d* core level spectra measured in different atmospheres in more detail. Figure 4(d) shows the relative contribution of the surface component estimated by the area of the high binding energy doublet in comparison to the total peak area. The more the probing depth is decreased, the more the areal contribution of the SrO surface component is increased in both atmospheres. This increase indicates a distinct surface termination or SrO coverage at the surface of the *n*-$SrTiO_3$ thin film for both ambient atmospheres. The overall contribution of the high binding energy doublet at a low base pressure (33% to 62%) is larger than at 1.3 mbar O_2 (27% to 45%). While opposite behavior has been reported in the literature when significant segregation of strontium from the bulk was observed [31,37,42,54], the observations here can be understood by a chemical response limited to the very surface region of the *n*-$SrTiO_3$ thin film, which implies atomic scale morphological rearrangements confined to the surface.

Based on the defect chemistry of *n*-$SrTiO_3$, Meyer *et al.* correlated the formation of surface charges in *n*-$SrTiO_3$ at temperatures of 1500 K to SrO precipitation from the bulk accompanied by the formation of strontium vacancies (V''_{Sr}) [30,31]. Such cation vacancies have a negative net charge. Formed at the surface, they may hence be responsible for the observed surface charge that drives electron depletion from the surface of *n*-$SrTiO_3$. Using Kroger-Vink notations [60], this surface reaction is described by

$$\tfrac{1}{2}O_2(g) + Sr^x_{Sr}(surf) + 2e^- \rightleftharpoons V''_{Sr}(surf) + (SrO)_{s.p.}. \quad (3)$$

While significant bulk dynamics of the Sr cation sublattice are limited to high temperatures [30,31], our results clearly indicate that a surface process attributed to the Sr sublattice is already active at temperatures of 670 K [41]. Due to the high diffusion times of Sr ions (at 670 K the Sr bulk diffusion length is about 1 Å within 24 hours) [31], the varying intensity of the SrO surface component may be related to a rearrangement of Sr ions at the surface, rather than to the exsolution of Sr ions from deeper regions. In fact, as we propose, a mere conversion of charge-neutral surface-terminating SrO units into extended precipitates can be responsible for the varied electron depletion, while consistently explaining the observed AP-XPS results.

TABLE I. Sheet carrier concentration, surface charge, and electric fields established in different oxygen atmospheres, as estimated from Fig. 5, for a temperature of 670 K.

	0.005 mbar O_2 (R_s)	1 mbar O_2 (R_s)
Sheet resistance R_s (kΩ)	78.3	83.9
Sheet carrier concentration n_s (cm^{-2})	1.76×10^{14}	1.65×10^{14}
Surface charge Q/A (e cm^{-2})	-2.88×10^{14}	-3.00×10^{14}
Electric field E (MV cm^{-1})	−4.30	−4.44

Figure 6 shows a schematic illustration of this surface redox process. At low pressure, one may assume a surface that is partially SrO terminated as a result of the growth process due to the incomplete growth of unit cells or slight nonstoichiometry [56,61]. In this case, the SrO coverage is charge neutral with respect to the lattice and is not accompanied by strontium vacancies at the surface [Fig. 6(a)]. Hence, this type of SrO coverage does not contribute a negative surface charge. Spectroscopically, however, this surface termination contributes to the core level doublet attributed to the SrO surface component at higher binding energy, rather than to the bulk contribution, due to the altered chemical bonding environment at the surface [37,54,55,62].

When increasing the oxygen pressure, the equilibrium of the surface reaction [Eq. (3)] is shifted to the right side [31]. Hence, the crystal lattice favors precipitating SrO and forming strontium vacancy defects, thereby increasing the surface defect concentration [Fig. 6(b)]. Due to the moderate temperatures, the described reaction is confined to the *n*-$SrTiO_3$ surface.

In the microscopic picture, an intuitive way to form surface strontium vacancies is the migration of strontium ions from surface-terminating SrO units on top of each other (as a first step of the nucleation of SrO), accompanied by the uptake of oxygen from the ambient atmosphere [Eq. (3)]. This process involves only a short migration length for strontium ions. Moreover, it is energetically favored as it minimizes the surface energy of the SrO precipitates, which have been shown to have a strong tendency to nucleate in the form of islands and not monolayers [37,54,56,63–68]. A further ripening of the SrO islands through coalescence is suppressed by the

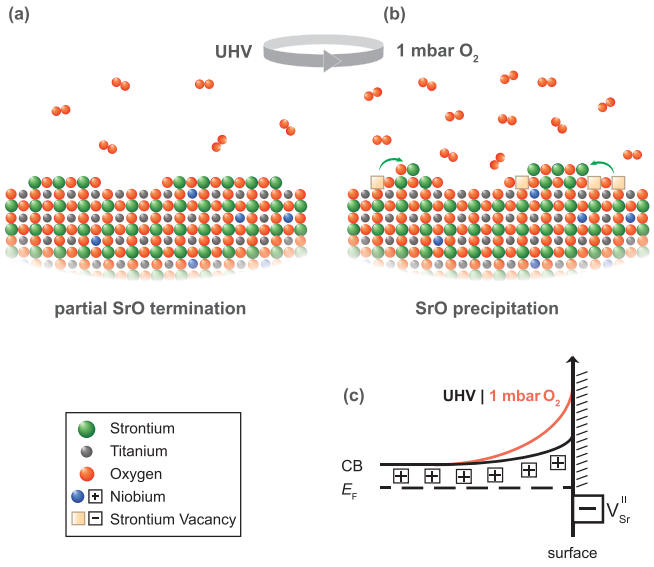

FIG. 6. Schematic illustration of the proposed surface redox chemistry of n-$SrTiO_3$ as the oxygen atmosphere is varied [(a), (b)]. The corresponding band diagram towards the surface is shown in (c). The variable negative ionic surface charge (−) provided by Sr vacancy defects is illustrated as a black box. Positive donor charges with the electron depletion layer at the surface layer are labeled as (+) signs.

low temperatures disabling the SrO movement on the surface. In this way, a transformation of the former SrO termination embedded into the $SrTiO_3$ lattice to more extended precipitates yields the formation of rocksalt-type SrO structures at the surface, leaving behind double negatively charged V''_{Sr} [Fig. 6(b)].

Island nucleation of the precipitated SrO also explains the higher overall contribution of the SrO doublet at low base pressures [Fig. 4(d)]. By increasing the pO_2, the amount of SrO unit cells located on top of each other increases [Fig. 6(b)], resulting in a lower total area occupation by SrO precipitates. Moreover, the contribution of buried SrO layers to the total intensity in XPS is reduced due to exponential attenuation of the emitted electrons. Hence, the total intensity of the SrO surface component at higher binding energies decreases with an increase in pO_2 (see also Sec. VI of the Supplemental Material [72]).

The altered negative surface charge provided by strontium vacancies formed at the surface drives electron depletion underneath the surface, corresponding to upwards band bending such as illustrated in Fig. 6(c). As the concentration of surface defects varies with oxygen pressure, also the band bending varies in response to the altered surface chemistry, causing stronger upwards band bending at higher oxygen pressure [Fig. 6(c)]. Note that consistent with the proposed scenario, previous reports based on scanning probe techniques have shown that changes of atomic surface reconstructions can already drive altered surface band bending [69–71], further supporting our findings.

Utilizing the surface charge determined from electrical characterization we can calculate the V''_{Sr} concentration needed to create the observed surface space charge layers. A single V''_{Sr} is double negatively charged. Hence, a V''_{Sr} surface concentration of 1.44×10^{14} cm^{-2} and 1.50×10^{14} cm^{-2} is required for 0.005 mbar and 1 mbar O_2, respectively, corresponding to vacancy concentrations of 23.0% and 24.0% within the first monolayer. Strontium vacancies are thus present at all tested conditions and cannot be removed even in UHV conditions. However, a rather subtle alteration of the V''_{Sr} concentration by just 1.0 percentage points leads to significant changes in the surface band bending and the corresponding electrical properties.

The ionic compensation of positive donor charge inside the layer via Sr vacancy defects is consistent with the classical defect chemistry of donor-doped $SrTiO_3$ favoring Sr vacancy formation over a wide range of oxygen activity, too [30,31]. The kinetic limitations that apply, however, suppress the formation of vacancy defects deep in the bulk of the thin films resulting in a spatial separation of negatively charged surface defects and positively charged donors in the adjacent electron depletion layer [Fig. 6(c)].

IV. CONCLUSIONS

We discussed the electrical surface properties of n-$SrTiO_3$ thin films showing significant electron depletion at their surface. Electron depletion is evident from (1) a thickness-dependent electron density, (2) a probing-depth-dependent binding energy shift of all characteristic core levels obtained from synchrotron-based AP-XPS, and (3) resistance relaxation experiments showing a response of electrical transport to a varied oxygen atmosphere. The latter experiments reveal a systematic pO_2 dependence of the electron depletion layer. Evidently, the surface space charge layer is present not only under oxidizing conditions at 1.3 mbar O_2 but also at a low base pressure of 10^{-8} mbar. Hence, even under vacuum conditions the electron depletion layer obtained at the surface of n-$SrTiO_3$ cannot be fully removed. Detailed Sr 3d core level analysis unveils a chemical surface response to a varied pO_2 with a major impact on the Sr chemistry at the surface. We propose clustering of SrO precipitates at the surface, leaving behind negatively charged strontium vacancies at the surface of n-$SrTiO_3$ as the origin of the surface space charge layer. In this way, a chemical control of the electrical properties of the thin film can be achieved by its redox chemistry. n-$SrTiO_3$ deliberately has to be treated as a material that shows severe band bending at its surface. This layer depends on pO_2 and can be diminished by a treatment in reducing conditions. However, it cannot by fully removed.

As we have demonstrated, surface and interface properties of doped transition metal oxides can be altered by exploiting their surface redox chemistry. Our results show that even subtle changes in the surface chemistry can cause significant changes in the electrical transport properties. Hence, growth as well as measurement atmosphere need to be selected and adjusted carefully, when addressing n-doped TMOs. This conclusion is important for the use of n-$SrTiO_3$ as a quasimetallic substrate material in highly oxidizing growth processes and also opens a new field of possible direct functionality. Particularly, similarly to surface properties addressed in this study, interface properties in n-$SrTiO_3$ will depend on the redox chemistry, too.

ACKNOWLEDGMENTS

The authors want to thank Jochen Friedrich for technical support and acknowledge the financial support of the W2/W3 program of the Helmholtz Association and DFG-GU1604 (No. 315025796). D.N.M. gratefully acknowledges support by the Juelich Joint Redox Laboratory (JJRL). This research used resources of the Advanced Light Source, which is a DOE Office of Science User Facility under Contract No. DE-AC02-05CH11231.

[1] C. Rao, Annu. Rev. Phys. Chern. **40**, 291 (1989).
[2] H. M. Christen and G. Eres, J. Phys.: Condens. Matter **20**, 264005 (2008).
[3] D. G. Schlom and J. Mannhart, Nat. Mater. **10**, 168 (2011).
[4] P. W. Anderson, Science (New York, NY) **177**, 393 (1972).
[5] R. Waser and M. Aono, Nat. Mater. **6**, 833 (2007).
[6] R. Waser, R. Dittmann, G. Staikov, and K. Szot, Adv. Mater. **21**, 2632 (2009).
[7] C. Baeumer, N. Raab, T. Menke, C. Schmitz, R. Rosezin, P. Müller, M. Andrä, V. Feyer, R. Bruchhaus, F. Gunkel, C. M. Schneider, R. Waser, and R. Dittmann, Nanoscale **8**, 13967 (2016).
[8] R. Dittmann, R. Muenstermann, I. Krug, D. Park, T. Menke, J. Mayer, A. Besmehn, F. Kronast, C. M. Schneider, and R. Waser, Proc. IEEE **100**, 1979 (2012).
[9] A. Ohtomo and H. Y. Hwang, Nature (London, UK) **427**, 423 (2004).
[10] F. Gunkel, S. Wicklein, S. Hoffmann-Eifert, P. Meuffels, P. Brinks, M. Huijben, G. Rijnders, R. Waser, and R. Dittmann, Nanoscale **7**, 1013 (2015).
[11] Z. Q. Liu, C. J. Li, W. M. Lü, X. H. Huang, Z. Huang, S. W. Zeng, X. P. Qiu, L. S. Huang, A. Annadi, J. S. Chen, J. M. D. Coey, T. Venkatesan, and Ariando, Phys. Rev. X **3**, 021010 (2013).
[12] G. Hodes, Science (New York, NY) **342**, 317 (2013).
[13] Y.-H. Huang, R. I. Dass, Z.-L. Xing, and J. B. Goodenough, Science (New York, NY) **312**, 254 (2006).
[14] A. Chroneos, B. Yildiz, A. Tarancón, D. Parfitt, and J. A. Kilner, Energy Environ. Sci. **4**, 2774 (2011).
[15] Y. Hikita, K. Nishio, L. C. Seitz, P. Chakthranont, T. Tachikawa, T. F. Jaramillo, and H. Y. Hwang, Adv. Energy Mater. **6**, 1502154 (2016).
[16] S. A. Chambers, Y. Du, R. B. Comes, S. R. Spurgeon, and P. V. Sushko, Appl. Phys. Lett. **110**, 082104 (2017).
[17] L. Kornblum, M. D. Morales-Acosta, E. N. Jin, C. H. Ahn, and F. J. Walker, Adv. Mater. Interfaces **2**, 1500193 (2015).
[18] F. Gunkel, R. Waser, A. H. H. Ramadan, R. A. De Souza, S. Hoffmann-Eifert, and R. Dittmann, Phys. Rev. B **93**, 245431 (2016).
[19] A. M. Schultz, T. D. Brown, and P. R. Ohodnicki, J. Phys. Chem. C **119**, 6211 (2015).
[20] R. Meyer and R. Waser, Sens. Actuators, B **101**, 335 (2004).
[21] A. G. Swartz, H. Inoue, T. A. Merz, Y. Hikita, S. Raghu, T. P. Devereaux, S. Johnston, and H. Y. Hwang, Proc. Natl. Acad. Sci. USA **115**, 1475 (2018).
[22] E. Mikheev, J. Hwang, A. P. Kajdos, A. J. Hauser, and S. Stemmer, Sci. Rep. **5**, 11079 (2015).
[23] C. Rodenbücher, T. Gensch, W. Speier, U. Breuer, M. Pilch, H. Hardtdegen, M. Mikulics, E. Zych, R. Waser, and K. Szot, Appl. Phys. Lett. **103**, 162904 (2013).
[24] J.-F. Ge, Z.-L. Liu, C. Liu, C.-L. Gao, D. Qian, Q.-K. Xue, Y. Liu, and J.-F. Jia, Nat. Mater. **14**, 285 (2015).
[25] V. Garcia, S. Fusil, K. Bouzehouane, S. Enouz-Vedrenne, N. D. Mathur, A. Barthélémy, and M. Bibes, Nature (London, UK) **460**, 81 (2009).
[26] A. Chanthbouala, A. Crassous, V. Garcia, K. Bouzehouane, S. Fusil, X. Moya, J. Allibe, B. Dlubak, J. Grollier, S. Xavier, C. Deranlot, A. Moshar, R. Proksch, N. D. Mathur, M. Bibes, and A. Barthélémy, Nat. Nanotechnol. **7**, 101 (2012).
[27] Z. Wen, D. Wu, and A. Li, Appl. Phys. Lett. **105**, 052910 (2014).
[28] K. J. May, D. P. Fenning, T. Ming, W. T. Hong, D. Lee, K. A. Stoerzinger, M. D. Biegalski, A. M. Kolpak, and Y. Shao-Horn, J. Phys. Chem. Lett. **6**, 977 (2015).
[29] R. Muenstermann, T. Menke, R. Dittmann, and R. Waser, Adv. Mater. **22**, 4819 (2010).
[30] R. Moos and K. H. Hardtl, J. Am. Ceram. Soc. **80**, 2549 (2005).
[31] R. Meyer, A. F. Zurhelle, R. A. De Souza, R. Waser, and F. Gunkel, Phys. Rev. B **94**, 115408 (2016).
[32] A. Ohtomo and H. Y. Hwang, Appl. Phys. Lett. **84**, 1716 (2004).
[33] Y. Kozuka, Y. Hikita, C. Bell, and H. Y. Hwang, Appl. Phys. Lett. **97**, 012107 (2010).
[34] A. Verma, A. P. Kajdos, T. A. Cain, S. Stemmer, and D. Jena, Phys. Rev. Lett. **112**, 216601 (2014).
[35] J. Son, P. Moetakef, B. Jalan, O. Bierwagen, N. J. Wright, R. Engel-Herbert, and S. Stemmer, Nat. Mater. **9**, 482 (2010).
[36] H. Inoue, M. Kim, C. Bell, Y. Hikita, S. Raghu, and H. Y. Hwang, Phys. Rev. B **88**, 241104(R) (2013).
[37] Z. Cai, M. Kubicek, J. Fleig, and B. Yildiz, Chem. Mater. **24**, 1116 (2012).
[38] R. A. De Souza, F. Gunkel, S. Hoffmann-Eifert, and R. Dittmann, Phys. Rev. B **89**, 241401(R) (2014).
[39] S. Sanna, V. Esposito, A. Tebano, S. Licoccia, E. Traversa, and G. Balestrino, Small **6**, 1863 (2010).
[40] S. Sanna, V. Esposito, J. W. Andreasen, J. Hjelm, W. Zhang, T. Kasama, S. B. Simonsen, M. Christensen, S. Linderoth, and N. Pryds, Nat. Mater. **14**, 500 (2015).
[41] M. Andrä, F. Dvořák, M. Vorokhta, S. Nemšák, V. Matolín, C. M. Schneider, R. Dittmann, F. Gunkel, D. N. Mueller, and R. Waser, APL Mater. **5**, 056106 (2017).
[42] A. Marchewka, D. Cooper, C. Lenser, S. Menzel, H. Du, R. Dittmann, R. E. Dunin-Borkowski, and R. Waser, Sci. Rep. **4**, 6975 (2015).
[43] M. Setvin, U. Aschauer, P. Scheiber, Y.-F. Li, W. Hou, M. Schmid, A. Selloni, and U. Diebold, Science **341**, 988 (2013).
[44] M. Setvín, B. Daniel, V. Mansfeldova, L. Kavan, P. Scheiber, M. Fidler, M. Schmid, and U. Diebold, Surf. Sci. **626**, 61 (2014).
[45] D. F. Ogletree, H. Bluhm, G. Lebedev, C. S. Fadley, Z. Hussain, and M. Salmeron, Rev. Sci. Instrum. **73**, 3872 (2002).

[46] D. Frank Ogletree, H. Bluhm, E. D. Hebenstreit, and M. Salmeron, Nucl. Instrum. Methods Phys. Res., Sect. A **601**, 151 (2009).
[47] S. Tanuma, C. J. Powell, and D. R. Penn, Surf. Interface Anal. **21**, 165 (1994).
[48] G. Johansson, J. Hedman, A. Berndtsson, M. Klasson, and R. Nilsson, J. Electron Spectrosc. Relat. Phenom. **2**, 295 (1973).
[49] V. Nefedov, Y. Salyn, G. Leonhardt, and R. Scheibe, J. Electron Spectrosc. Relat. Phenom. **10**, 121 (1977).
[50] P. Blennow, A. Hagen, K. K. Hansen, L. R. Wallenberg, and M. Mogensen, Solid State Ionics **179**, 2047 (2008).
[51] A. V. Kovalevsky, M. H. Aguirre, S. Populoh, S. G. Patrício, N. M. Ferreira, S. M. Mikhalev, D. P. Fagg, A. Weidenkaff, and J. R. Frade, J. Mater. Chem. A **5**, 3909 (2017).
[52] K. K. Adepalli, J. Yang, J. Maier, H. L. Tuller, and B. Yildiz, Adv. Funct. Mater. **27**, 1700243 (2017).
[53] F. V. E. Hensling, C. Xu, F. Gunkel, and R. Dittmann, Sci. Rep. **7**, 39953 (2017).
[54] K. Szot, W. Speier, U. Breuer, R. Meyer, J. Szade, and R. Waser, Surf. Sci. **460**, 112 (2000).
[55] T. Hara, T. Ishiguro, and K. Shinozaki, Jpn. J. Appl. Phys. **49**, 09MA15 (2010).
[56] C. Baeumer, C. Xu, F. Gunkel, N. Raab, R. A. Heinen, A. Koehl, and R. Dittmann, Sci. Rep. **5**, 11829 (2015).
[57] A. Shavorskiy, X. Ye, O. Karslıoğlu, A. D. Poletayev, M. Hartl, I. Zegkinoglou, L. Trotochaud, S. Nemšák, C. M. Schneider, E. J. Crumlin, S. Axnanda, Z. Liu, P. N. Ross, W. Chueh, and H. Bluhm, J. Phys. Chem. Lett. **8**, 5579 (2017).
[58] Note that discharging of the sample surface by electrons generated through ionization of gas phase molecules by the incident photon beam can be neglected due to the high conductivity of our thin film (see Sec. III C).
[59] T. Higuchi, T. Tsukamoto, N. Sata, M. Ishigame, Y. Tezuka, and S. Shin, Phys. Rev. B **57**, 6978 (1998).
[60] F. Kröger and H. Vink, Solid State Phys. **3**, 307 (1956).
[61] C. Baeumer, C. Schmitz, A. H. H. Ramadan, H. Du, K. Skaja, V. Feyer, P. Müller, B. Arndt, C.-L. Jia, J. Mayer, R. A. De Souza, C. Michael Schneider, R. Waser, and R. Dittmann, Nat. Commun. **6**, 8610 (2015).
[62] C. Rodenbücher, S. Wicklein, R. Waser, and K. Szot, Appl. Phys. Lett. **102**, 101603 (2013).
[63] B. Rahmati, J. Fleig, W. Sigle, E. Bischoff, J. Maier, and M. Rühle, Surf. Sci. **595**, 115 (2005).
[64] Y. F. Nie, Y. Zhu, C.-H. Lee, L. F. Kourkoutis, J. A. Mundy, J. Junquera, P. Ghosez, D. J. Baek, S. Sung, X. X. Xi, K. M. Shen, D. A. Muller, and D. G. Schlom, Nat. Commun. **5**, 4530 (2014).
[65] J. H. Lee, G. Luo, I. C. Tung, S. H. Chang, Z. Luo, M. Malshe, M. Gadre, A. Bhattacharya, S. M. Nakhmanson, J. A. Eastman, H. Hong, J. Jellinek, D. Morgan, D. D. Fong, and J. W. Freeland, Nat. Mater. **13**, 879 (2014).
[66] Y. Chen, H. Téllez, M. Burriel, F. Yang, N. Tsvetkov, Z. Cai, D. W. McComb, J. A. Kilner, and B. Yildiz, Chem. Mater. **27**, 5436 (2015).
[67] J. Druce, H. Téllez, M. Burriel, M. D. Sharp, L. J. Fawcett, S. N. Cook, D. S. McPhail, T. Ishihara, H. H. Brongersma, and J. A. Kilner, Energy Environ. Sci. **7**, 3593 (2014).
[68] H. Dulli, P. A. Dowben, S.-H. Liou, and E. W. Plummer, Phys. Rev. B **62**, 14629(R) (2000).
[69] M. S. J. Marshall, A. E. Becerra-Toledo, L. D. Marks, and M. R. Castell, Phys. Rev. Lett. **107**, 086102 (2011).
[70] S. Gerhold, Z. Wang, M. Schmid, and U. Diebold, Surf. Sci. **621**, L1 (2014).
[71] A. E. Becerra-Toledo, M. S. J. Marshall, M. R. Castell, and L. D. Marks, J. Chem. Phys. **136**, 214701 (2012).
[72] See Supplemental Material at http://link.aps.org/supplemental/10.1103/PhysRevMaterials.3.044604 for more information on the growth process, further experimental results, and an abstract discussion of the influence of the space charge layer on the spectroscopic analysis.